Surface Modification of Titanium by Femtosecond Laser in Reducing Bacterial Colonization

Xinhui Wu [1], Haiyong Ao [2], Zhaoru He [3], Qun Wang [4] and Zhaoxiang Peng [1,*]

1   The Affiliated Lihuili Hospital, School of Medicine, Ningbo University, Ningbo 315100, China; wuxinhui1996@163.com
2   Jiangxi Key Laboratory of Nanobiomaterials, Institute of Advanced Materials, East China Jiaotong University, Nanchang 330000, China; aohyong@126.com
3   College of Materials Science and Technology, Nanjing University of Aeronautics and Astronautics, Nanjing 210016, China; hezhaoru@nuaa.edu.cn
4   Key Laboratory of Impact and Safety Engineering, School of Mechanical Engineering and Mechanics, Ningbo University, Ningbo 315211, China; wangqun_yz@163.com
*   Correspondence: pzxao@hotmail.com

Abstract: In the past few decades, titanium and its alloys have been widely used in the orthopaedic field. However, because titanium is bioinert and lacks antibacterial properties, infection may happen when bacteria attach to implant surfaces and form biofilms. It has been studied that some naturally existing micron-scale topographies can reduce bacterial attachment such as cicada wings and gecko skins. The aim of this in vitro study was to find an implant with good biocompatibility and antimicrobial properties by the modification of micron-scale topographies. In this paper, a femtosecond laser was used to provide microtopography coatings on Ti substrates. The surface morphology of Ti substrates was observed by scanning electron microscopy (SEM). XPS was used to fulfil the chemical compositional analysis. The surface wettability was measured by contact angle measurement system. The effect of microtopography coatings with different surface microstructures on bacterial activities and bone marrow mesenchymal stem cells (BMSC) functions was investigated. The results of in vitro study revealed that microtopography coatings restrain the adhesion of *Staphylococcus aureus* (*S. aureus*) and *Staphylococcus epidermidis* (*S. epidermidis*), which are common pathogens of orthopaedic implant infections. In addition, microtopography coatings stimulated BMSC adhesion and proliferation. Our studies suggest that a microtopography-coated sample modified by femtosecond laser showed promising antibacterial properties and favourable biocompatibility. The femtosecond laser technique provides an accurate and valid way to produce microtopography coatings with outstanding biocompatibility and antimicrobial properties, and could be widely used to modify the surface of orthopaedic metal implants with great potential.

Keywords: femtosecond laser; surface modification; microtopography; antimicrobial activity; biocompatibility

1. Introduction

Over the past few decades, implants have been widely used in various orthopaedic surgeries. As a kind of biocompatible metal with corrosion resistance, nontoxicity, and appropriate mechanical properties, titanium (Ti) has become the most popular orthopaedic implant material [1]. Nevertheless, orthopaedic implant surgery may fail when orthopaedic implant infection happens as a result of pathogens attaching to implant surfaces and forming biofilms [2,3]. According to statistics, the incidence of orthopaedic implant infection reaches 2–5% [4]. In recent years, a lot of research about chemical modification on implant surfaces has been performed. For example, silver nanoparticle technology shows excellent antimicrobial properties in the field of orthopaedics [5,6], and antibiotic-coated implants also play a role in killing bacteria [7,8]. However, at present, the toxic effects of

silver nanoparticles on mammalian cells have attracted attention [9], antibiotics may cause a problem of drug-resistant bacteria [10] and may also affect the biocompatibility of an implant in the meantime [11], so the use of an antibiotic-coated implant is also limited. For a successful implant, strong antimicrobial activity and appropriate biocompatibility are essential; as such, it is necessary to design implants that satisfy both in the same time.

A large number of studies prove that micron-scale topographies affect the attachment and biofilm formation of different bacterial strains [12–17]. These studies indicate that producing micron-scale topographies on implant surfaces can endow implants with the capacity to inhibit early bacterial adhesion. On the other hand, no chemicals are used in the process of producing micron-scale topographies, which means that the biocompatibility can be maintained. However, it is worth mentioning that the size and shape of micron-scale topographies both have a great influence on bacterial attachment.

Many topographic patterns have been proved to restrain bacterial adhesion, such as micro holes [12], line patterns [18], and ridges patterns [19]; this shows that it is important to design patterns of topographies wisely. What is more, some naturally existing micron-scale topographies can reduce bacterial attachment such as cicada wings and gecko skins [20–22].

Taking all these into consideration, microtopography coating by mimicking naturally existing micron-scale topographies presents an attractive way to strengthen the antimicrobial property and biocompatibility of the implant.

Various techniques have been employed to prepare topographies [23–25], but these processes do not provide well-defined surface topographies. Additionally, research has shown that rationally designed topography can reduce more bacterial attachment [26]. So, selecting an accurate and controllable way to fulfil the design of microtopography coating is necessary. Femtosecond laser possesses several advantages in the field of processing metal material, such as high instantaneous power, low thermal effects, high precision, and high stability, which are perfectly suitable for producing bionic microtopography coatings.

In order to find out the physical and chemical characteristics of a sample surface, SEM, XPS, and contact angles measurements are conducted. SEM is considered to be the best way to observe the surface morphology. The effects of XPS include chemical elements qualitative analysis and chemical elements quantitative analysis, and we can figure out elemental changes after the processing of femtosecond laser. Wettability is usually measured by contact angles, so that contact angles measurements are also chosen. As for in vitro study, *S. aureus* and *S. epidermidis* were chosen for they are the most frequently detected pathogens in infections on implants [27,28], we can assume that microtopography coating may reduce the incidence of infection if they show antimicrobial properties towards *S. aureus* and *S. epidermidis*. According to research before, bone marrow mesenchymal stem cells (BMSC) have important biological properties and play an essential role in tissue healing, modulating the production of important cytokines. Additionally, BMSC also accelerates bone regeneration and has angiogenic potential [29]; it is of great benefit if BMSC adhere and multiply well on microtopography coatings. So, BMSC was chosen to be our experimental cell.

In this study, four kinds microtopography coatings with different surface microstructures were prepared by femtosecond laser. The surface morphology, surface wettability, and surface composition of the samples were measured. The antibacterial properties of the bionic microtopography coatings against *Staphylococcus aureus* (*S. aureus*) and *Staphylococcus epidermidis* (*S. epidermidis*) were determined and the cellular biological effects with Bone marrow mesenchymal stem cells (BMSC) were studied.

2. Materials and Methods

2.1. Bionic Microtopography Coatings Sample Preparation

Titanium alloy (Baoji Titanium Industry Co., Ltd., Baoji, China) was prepared by a wire cutting process and then metallography sandpaper of #320, #600, #800, #1000, and #1500 were used to polish the surface of titanium alloy. Before laser treatment, the titanium alloy surface was cleaned with acetone (Mianyang Rongsheng Chemical Reagent Co.,

Ltd., Mianyang, China) and ethanol (Sinopharm Chemical Reagent Co., Ltd., Beijing, China), respectively, then cleaned by ultrasonic bath (Front Ultrasonic Technology Co., Ltd., Hangzhou, China) for 10 min, and dried in an oven(Puruisi Co., Ltd., Suzhou, China) at 100 °C for 30 min. The laser used in this work is a laser system (TruMicro 5050, TRUMPF, Ditzingen, Germany) at λ = 1030 nm and repetition rate = 50 kHz. The pre-treated samples were textured by a femtosecond laser which generated 40 femtoseconds (fs) laser pulses by focusing the laser beam on the surface of the target. The laser beam was scanned over the sample in rectangular pattern by irradiating the sample in the horizontal direction (0°) and then along the vertical direction (90°) in order to create grid patterns. The distance between two adjacent lines was 100 μm. The diameter of the focused spot on the surface was 100 μm. All samples were prepared under standard atmospheric pressure in an open atmosphere at ambient temperature. In order to explore the influence of different surface structures on surface properties, four different surface microstructures were designed and prepared, including (group a) groove pattern, (group b) micro-hole pattern, (group c) directional grain pattern, and (group d) stripe pattern, while ordinary titanium without surface microstructures was used as (group e) control group. Finally, the samples were cleaned by ultrasonic ethanol bath for 10 min to remove the debris.

2.2. Surface Characterization

2.2.1. Surface Morphology Measurements

All the samples were thoroughly rinsed with deionized water and then dried at room temperature. The surface morphology of the samples was characterized by scanning electron microscopy (Hitachi S-4800, Hitachi, Tokyo, Japan).

2.2.2. Chemical Composition Measurements

Chemical compositional analysis was analysed by XPS (ESCALAB 250XI, Thermo Scientific, Waltham, MA, USA).

2.2.3. Wettability Measurements

The surface wettability was measured by contact angles. Contact angle measurements were conducted and analysed by Contact Angle Measurement System (SEO Phoenix 300, SEO, Seoul, Korea). One droplet (4 μL) of deionized water was added on top of the substrates. The contact angle was immediately measured 5 s after placing the drop on each sample and the test was conducted at room temperature. Measurements were performed three times; the average contact angle was determined.

2.3. Antimicrobial Assays

2.3.1. Bacterial Inhibitory Assays

Bacteria cell lines of S. aureus (ATCC6538), and S. epidermidis (CMCC(B)26069) were used in this study. All sterilized samples were transferred into 48 well culture plates and rinsed twice with phosphate-buffered saline (PBS). Then, the samples were treated with the prepared bacterial solutions at a concentration of 1×10^6 bacteria/mL in tryptic soy broth (TSB, 0.03 g/mL) and cultured for 6 h in an incubator (Heratherm, Thermo Scientific, Waltham, MA, USA) at 37 °C, humidified, 5% CO_2. Afterward, the samples were washed twice with PBS to remove the floating bacteria and were transferred into 15 mL tubes with 3 mL of PBS each. Following this, the samples were sonicated for 10 min to release the bacteria attached on the sample surface into the PBS solution. Then, a series of diluted solutions with bacteria were pipetted onto TSB agar plates and bacteria colonies were counted after 24 h of incubation.

2.3.2. Confocal Laser Scanning Microscopy (CLSM) Assays

Samples were prepared and seeded with bacterial solutions as already described. After 6 h of incubation, the samples were washed three times with PBS and then stained by LIVE/DEAD BacLight bacterial viability kits (L7012, Thermos Fisher Scientific, Waltham,

MA, USA) for 15 min at room temperature in the dark. Following this, samples were subsequently analysed with a confocal laser scanning microscope (Leica TCS SP8, Leica, Heidelberg, Germany). The viable and nonviable cells can be distinguished under the fluorescence microscope because the viable bacteria with intact cell membranes appear fluorescent green, whereas nonviable bacteria with damaged membranes appear fluorescent red. The Leica confocal software was used to analyse the biofilm images. The images were acquired from random positions on the surface of the cement discs.

2.3.3. Scanning Electron Microscopy (SEM) Assays

After cultured with bacterial solutions for 6 h, the samples were washed three times with PBS and were fixed in 2.5% glutaraldehyde for 2 h at 4 °C then washed three times with cacodylate buffer and dehydrated through a series of graded ethanol solutions (25, 50, 75, 95 and 100%). The samples were subsequently freeze-dried, sputter coated with gold, and observed using a scanning electron microscope (HIROX, Merlin, Tokyo, Japan).

2.4. Cell Assays
2.4.1. Cell Culture

Bone marrow mesenchymal stem cells (BMSC) were used for all cell experiments. All cells were cultured in bone marrow mesenchymal stem cell complete medium, and were cultured at 37 °C in a humidified, 5% CO2/95% air environment (CI191C, Thermos Fisher Scientific, Waltham, MA, USA).

2.4.2. Cell Viability Assays

For cell viability assays, all the sterilized Ti samples were placed individually into the wells of 24 well tissue culture plates. Samples were rinsed twice with PBS. After this, cells were seeded onto the samples at a density of 1×10^4 cells/cm^2. Cytotoxicity was measured after 1, 3, and 5 days of culture. The medium was changed every other day during proliferation trials. After the prescribed incubation time, CCK-8 dye was added to each well, then the plates were cultured for another 4 h at 37 °C. At last, the optical density (OD) was measured at 450 nm by a plate reader.

2.4.3. Adhesion and Proliferation Assays

Before proliferation assays, FITC and DAPI were prepared as described in the instruction manual. Samples were prepared and seeded with cells after 1, 3, and 5 days of culture as already described. Abandon the medium and wash the samples with PBS twice. The cells were fixed in 4% paraformaldehyde for 30 min and then cultured with Triton X-100 for 10 min. After this, all cells were cultured with FITC for 5 min to stain F-actin which indicated the cell skeleton, and 30 min with DAPI to mark the core. Finally, samples were subsequently analysed with a confocal laser scanning microscope (Leica TCS SP8, Leica, Heidelberg, Germany). The Leica confocal software was used to analyse the biofilm images. The images were acquired from random positions on the surface of the cement discs.

2.5. Statistical Analysis

All cell and bacteria studies were conducted in triplicate and repeated at least three times. Data were collected and the significant differences were assessed using ANOVA followed by one-tailed Student's *t*-tests. Statistical significance was considered at $p < 0.05$.

3. Results

3.1. Surface Characterization

3.1.1. Surface Morphology

Morphological characterization of the sample surface observed by SEM was shown in Figure 1a–d. Microtopography coatings are basically obtained as designed. Grooves with equal length, equal width, and equal spacing can be observed in groove pattern (Figure 1a), while the length, width, and spacing of the grooves were 20, 5, and 15 μm, respectively. Compact and regularly arranged micro-holes can be observed in micro-hole pattern (Figure 1b), the diameter of each micro-hole was 5 μm, spacing between holes was 20 μm. As shown in (Figure 1c), directional grain pattern contains several directionally arranged orthogonal grain, the length of each edge was 25 μm and spacing between each grain is 5μm. The length of stripes (Figure 1d) vary from 12 to 20 μm, the width is 5 μm, they are first incremental then diminishing arranged according to the length.
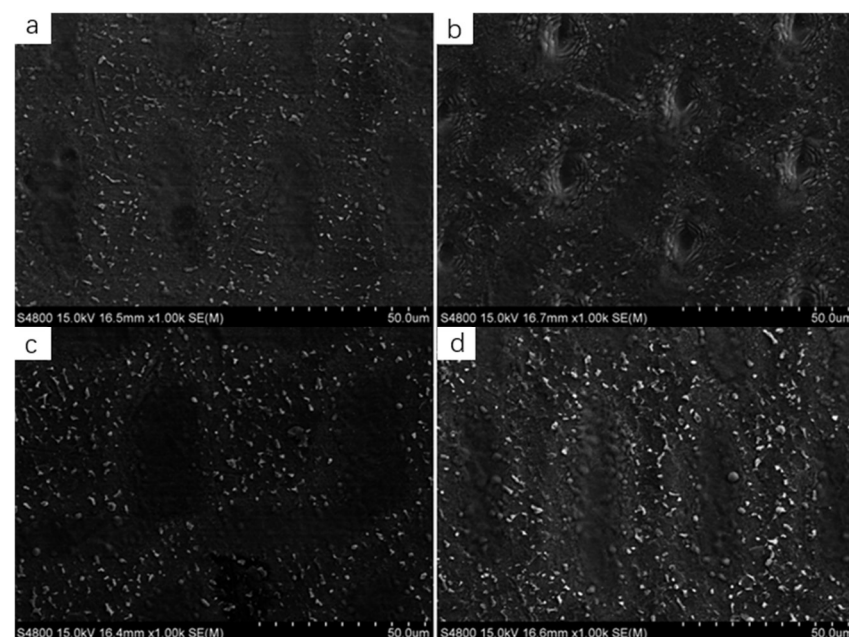
**Figure 1.** SEM images of surface morphology: (**a**) groove pattern; (**b**) micro-hole pattern; (**c**) directional grain pattern; (**d**) stripe pattern. Abbreviations: SEM, scanning electron microscopy.

3.1.2. Chemical Composition

To study the chemical composition of the samples, the samples were analysed by XPS, and all of their spectra were presented in Figure 2a–d.

Figure 2a,b show the survey XPS spectrum and Ti2p XPS spectrum of the samples, respectively [30]. There are three obvious peak changes on the sample surface before and after processing. The binding energy peaks near 1090 eV and 500 eV decreased greatly after processing, while two peaks increased greatly near 100 eV and 150 eV. Figure 2c,d show the O1s and Al2p XPS spectra of the samples [31]. After processed by femtosecond laser, the peak intensity of oxygen increased significantly from 108,458 eV to 145,100 eV, and the impurity peak in the XPS spectrum of O1s disappears. Combined with the diagram of Al2p, we can know that the peak intensity of Al decreases from around 4500 eV to around 2500 eV.
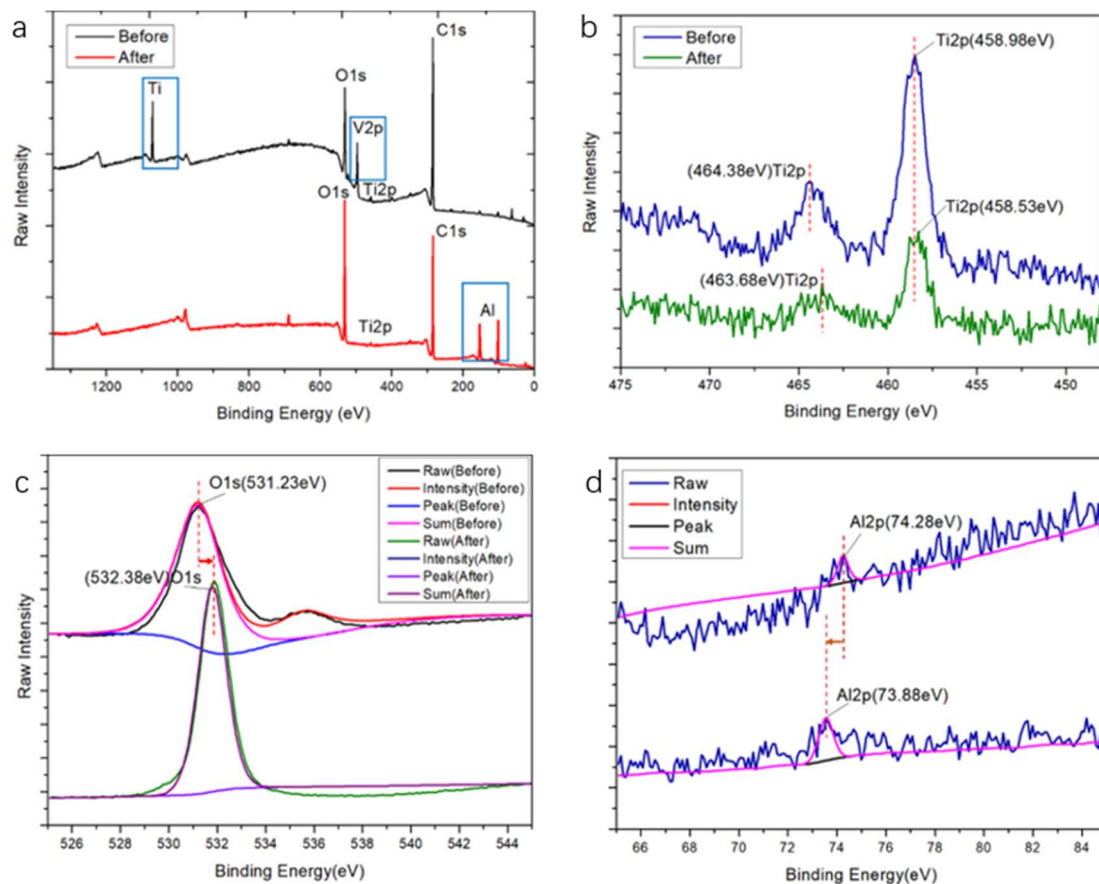
Figure 2. XPS patterns of the samples with different bionic microtopography coatings. Notes: (**a**) survey XPS spectrum; (**b**) Ti2p XPS spectrum; (**c**) O1s XPS spectrum; (**d**) Al2p XPS spectrum.

3.1.3. Surface Wettability

Figure 3 shows the water contact angle images, and Table 1 lists the average contact angle for the five groups. The largest average water contact angle is 141.6°, on the surface of the (b) micro-hole pattern. The smallest contact angle was observed from the (d) stripe pattern, approaching 76.2°. The water contact angle of (a) groove pattern and (c) directional grain pattern is 79.5° and 78.7°. The water contact angle of group B is significantly larger than Ti control group, while the water contact angle of group a, group c, and group d have no significant differences compared to that of Ti control group and there are no significant differences between group a, group c, and group d.

Table 1. The average water contact angle of (**a**) groove pattern; (**b**) micro-hole pattern; (**c**) directional grain pattern; (**d**) stripe pattern (**e**) control group.

Substrates	Surface Wettability (Water Contact Angle/°)
a	79.5°
b	141.6°
c	78.7°
d	76.2°
e	78°

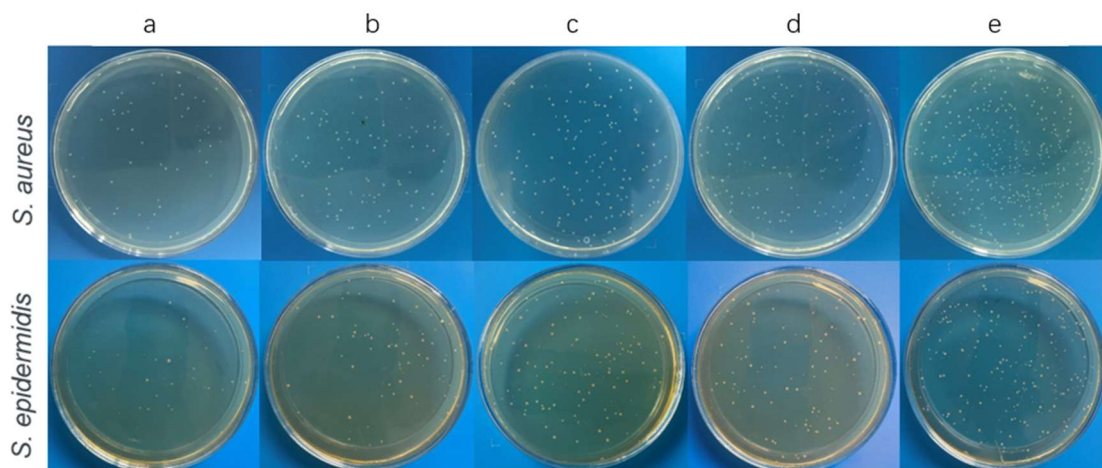Notes: Data represent mean $\pm$ SD, N = 3.
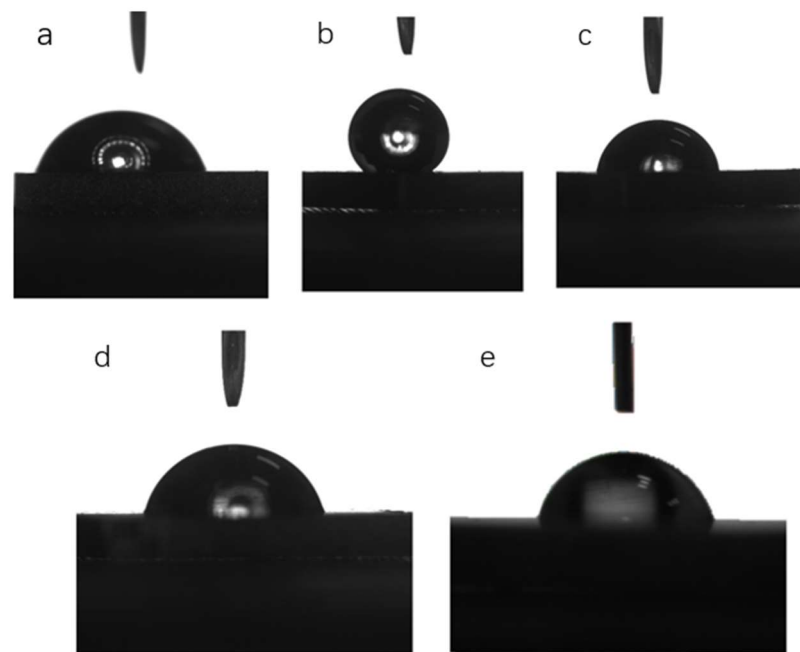
Figure 3. Schematic of the water contact angle of (**a**) groove pattern; (**b**) micro-hole pattern; (**c**) directional grain pattern; (**d**) stripe pattern (**e**) control group.

3.2. Antimicrobial Assays

3.2.1. Bacterial Inhibitory Assays

The antibacterial properties of the microtopography coatings against *S. aureus* and *S. epidermidis* were determined. As shown in Figures 4 and 5, the amount of bacterial colony from microtopography coating samples is significantly less than that from Ti group, which indicated that the bionic microtopography coating samples inhibited the adhesion and growth of these two kinds of bacteria compared with Ti control.
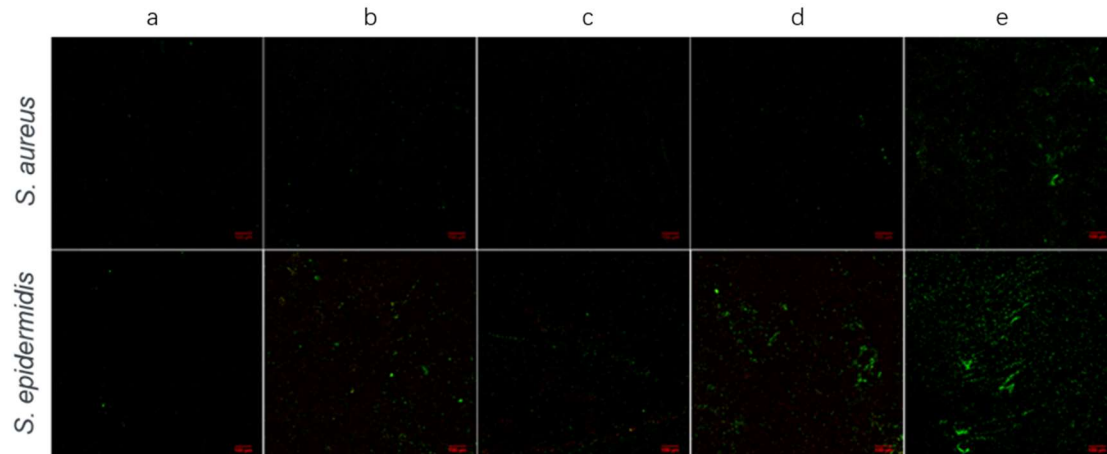

Figure 4. Typical images of re-cultivated *S. aureus* and *S. epidermidis* colonies from the samples after 6 h incubation. Notes: (**a**) groove pattern; (**b**) micro-hole pattern; (**c**) directional grain pattern; (**d**) stripe pattern (**e**) control group.
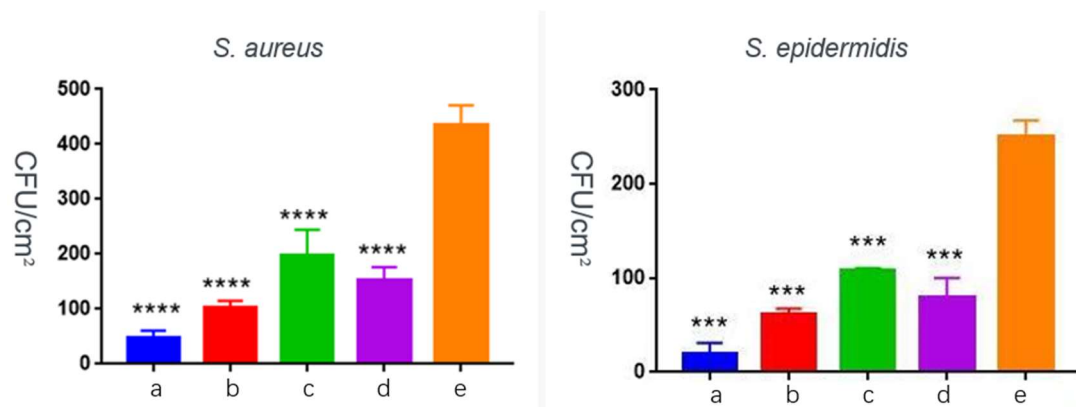
Figure 5. *S. aureus* and *S. epidermidis* growth on samples with different coatings after 6 h incubation. Data represent mean $\pm$ SD, N = 4. *** $p < 0.001$, **** $p < 0.0001$ compared with Ti control. Notes: (**a**) groove pattern; (**b**) micro-hole pattern; (**c**) directional grain pattern; (**d**) stripe pattern (**e**) control group.

3.2.2. Confocal Laser Scanning Microscopy (CLSM) Assays

To further study the antibacterial properties of the microtopography coatings, the formation of bacterial biofilms was observed by confocal laser scanning microscopy. Green fluorescence represents live bacteria, while red fluorescence represents dead bacteria. It is clear that live bacteria on microtopography coatings were greatly inhibited compared with those on Ti control (Figure 6). What is more, red fluorescence can be seen on every group of bionic microtopography-coated sample.
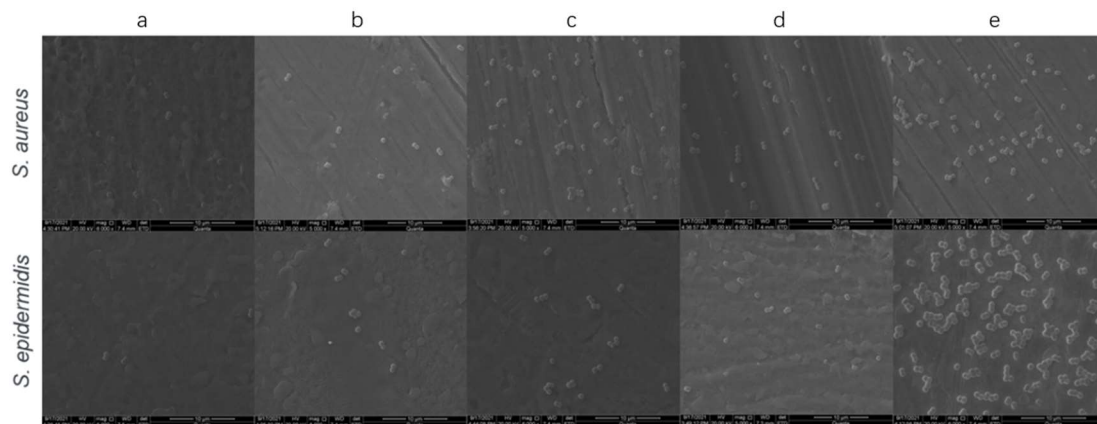

Figure 6. CLSM images of *S. aureus* and *S. epidermidis* colonies on samples with different coatings after 6 h incubation. Notes: (**a**) groove pattern; (**b**) micro-hole pattern; (**c**) directional grain pattern; (**d**) stripe pattern (**e**) control group. Abbreviations: CLSM, confocal laser scanning microscopy.

3.2.3. Scanning Electron Microscopy (SEM) Assays

SEM was also used to examine bacteria attachment on the sample surfaces (Figure 7). After colonization with the two tested strains, samples with each kind of microstructure contain much fewer colonies than Ti control sample, suggesting that bacterial biofilm may grow better on Ti control surface. We noticed that there is hardly any colony observed on group a, suggesting that samples with groove pattern bionic microstructures possess the strongest antibacterial property, which is consistent with the previous results (Figures 4–6).

Figure 7. SEM images of *S. aureus* and *S. epidermidis* colonies on samples with different coatings after 6 h incubation. Notes: (**a**) groove pattern; (**b**) micro-hole pattern; (**c**) directional grain pattern; (**d**) stripe pattern (**e**) control group. Abbreviations: SEM, scanning electron microscopy.

### 3.3. Cell Assays

3.3.1. Cell Viability Assays

CCK-8 assay kit was adopted to evaluate the viability of microtopography-coated sample; the result is shown in Figure 8. After incubation for 1 d, the OD value of cells on the bionic microtopography-coated sample was higher than that on the Ti control, of which the OD value of group a and group d was significantly higher. After incubation for 3 d, the OD value of the microtopography-coated sample was significantly higher than that of the Ti control. After 5 d, the OD value of cells on the microtopography-coated sample was higher than that on the Ti control, of which the OD values of group a, group c, and group d were significantly higher.
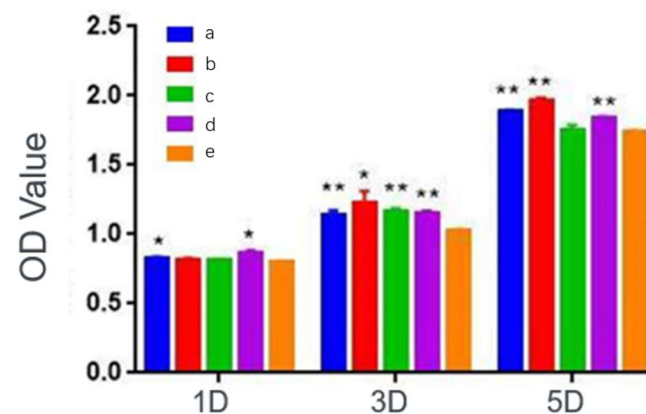
Figure 8. OD value after 1, 3, and 5 days of culture with bone marrow mesenchymal stem cells (BMSC). Notes: (**a**) groove pattern; (**b**) micro-hole pattern; (**c**) directional grain pattern; (**d**) stripe pattern (**e**) control group. Abbreviations: OD, optical density, * $p < 0.1$, ** $p < 0.01$.

3.3.2. Adhesion and Proliferation Assays

To estimate the cell adhesion and proliferation on the microtopography-coated sample, CLSM was used to observe the number and morphology of the cells (Figure 9). The cell skeleton showed green fluorescence stained by FITC and the cell core showed blue fluorescence stained by DAPI. After incubation for 1d, viable BMSC appeared on all sample surfaces after incubation, the number of viable cells increased predominantly after incubation for 3 d and further became enormously larger 5d later. Furthermore, the well extended and elongated cytoskeleton was observed obviously on all sample surfaces after incubation for 3 d and 5 d.
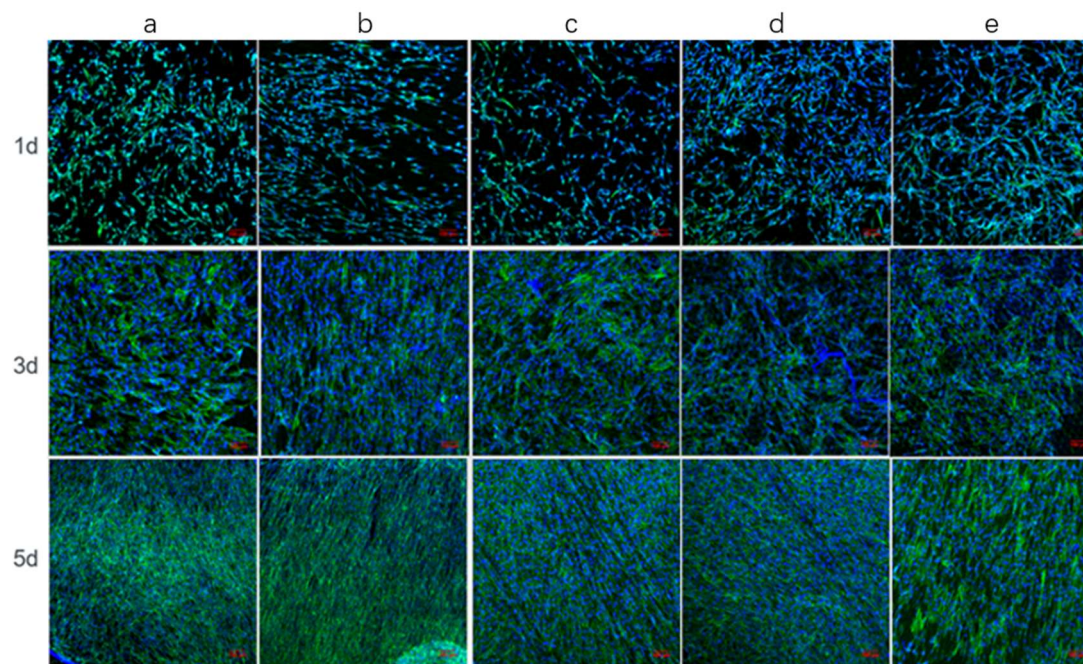
Figure 9. CLSM image of sample surface after cultured for 1, 3, and 5 days with bone marrow mesenchymal stem cells (BMSC). Notes: (**a**) groove pattern; (**b**) micro-hole pattern; (**c**) directional grain pattern; (**d**) stripe pattern (**e**) control group. Abbreviations: CLSM, confocal laser scanning microscope.

4. Discussion

As orthopaedic implant infection starts with the adhesion of pathogens and the formation of biofilms while implant surfaces play a vital importance in affecting initial biological events, it is meaningful to develop a kind of implant with strong antimicrobial activity and appropriate biocompatibility. It has been studied that some naturally existing micron-scale topographies can reduce bacterial adhesion. Inspired by that, femtosecond laser was chosen to produce microtopography coatings for its precision and stability.

In this study, four different microtopography coatings with different surface microstructures were designed and prepared by femtosecond laser, including (group a) groove pattern, (group b) micro-hole pattern, (group c) directional grain pattern, and (group d) stripe pattern, while ordinary titanium without surface microstructures was used as (e) control group.

Surface microstructures observed by SEM (Figure 1a–d) indicated that microtopography coatings are basically obtained as designed, suggesting that femtosecond laser technology is a qualified method to modify the surface of titanium and build micron-scale topographies accurately, which is consistent with previous research [32–34]. In order to study the chemical composition of the samples, the samples were analysed by XPS (Figure 2a–d). Combine the result that peak intensity of oxygen increasing (Figure 2c) with the result that peak intensity of impurity disappears (Figure 2a), it can be inferred that the processing removed the original impurity and formed new metal oxide film. No element was introduced into the surface during the processing. The surface wettability was measured by contact angles. As shown in Figure 3 and Table 1, average water contact angle of Ti control was smaller than that of micro-hole pattern (Figure 3b) while having no difference from that of groove pattern (Figure 3a), directional grain pattern (Figure 3c), and stripe pattern (Figure 3d), which was indicated as hydrophobic for group B. These findings are consistent with many previous studies that some micron-scale topographies can weaken the surface wettability as a result of Cassie State [35].

Once the surfaces characterization was accomplished, antimicrobial activity of these microtopography coatings were examined. *S. aureus* and *S. epidermidis* were chosen in this

study for they are the most frequently detected pathogens in infections on implants [27,28]. The amount of bacterial colony from microtopography coating samples is significantly less than that from Ti group, suggesting that these four kinds microtopography coating do have antimicrobial activity as expected. To further study the mechanism of the antimicrobial activity from microtopography coating, CLSM and SEM was also used. SEM image revealed that samples with microtopography coating contain much fewer colonies than the Ti control sample, which means microtopography coating inhibits the bacterial adhesion. CLSM image (Figure 7) not only manifested weaker green fluorescence, which means fewer formation of bacterial films, but also red fluorescence representing dead bacteria. Taking all this together, microtopography coatings not only restrained bacterial adhesion but also killed the bacteria to a certain extent. The capacity to inhibit bacterial adhesion could be attributed presumably to microtopography. Micron-scale topographies have been reported to disturb the bacterial adhesion by affecting bacteria-surface interactions [36,37]; in this study, we assume these four different microtopography coatings affect bacteria-surface interactions by blocking the bacterial biofilm formation. The diameter of *S. aureus* and *S. epidermidis* is about 1 μm, while four different surface microstructures we obtained are also micron-sized so that bacteria may not able to multiply into colony and form bacterial biofilm. Once the formation of bacterial biofilm is blocked, the amount of bacteria able to adhere to the sample surface is also limited. The capacity to kill the bacteria may be an effect from metal oxides formed during femtosecond laser processing. It has been reported that the photoactivated titanium dioxide could result in the destruction of bacteria [38,39].

An ideal orthopaedic implant should not only have strong antimicrobial activity but also appropriate biocompatibility. Considering that, cell viability, adhesion, and proliferation assays have been performed. For cell viability assays, the OD value of cells on microtopography-coated samples was all higher or indiscriminate compared with Ti group after incubation for 1, 3, and 5d. For adhesion and proliferation assays, the well extended and elongated cytoskeleton was observed obviously on all sample surface after incubation for 3d and 5d by CLSM. It is obvious that there are no significant differences about cell proliferation between bionic microtopography-coated samples and Ti control, suggesting that microtopography-coated samples possess the same ability to promote cell adhesion as Ti control. To sum up, microtopography coating does no harm to the biocompatibility. The good biocompatibility of group a, group c, and group d is predictable which is in agreement with previous reports indicating that good wettability results in good biocompatibility [40–42]. It is a surprise that group b also exhibits fine biocompatibility with hydrophobic; a possible explanation is that micron-scale topographies will affect cell adhesion and proliferation not only by changing the wettability of surface but also manipulating the cell–surface interactions by providing a 3D landscape for cells which is more biologically relevant [43,44].

As a limitation, this study only investigated the antimicrobial properties and biocompatibility in vitro, and there is no evidence that the antimicrobial properties and biocompatibility will remain in the complex environment of living bodies. As a future study, an in vivo model is required to research the possible infection after these microtopography-coated samples are implanted into living bodies.

5. Conclusions

Microtopography coatings on Ti-based implants using the femtosecond laser technique showed promising antimicrobial activity toward *S. aureus* and *S. epidermidis*, which are the common pathogens of orthopaedic implant infection. In addition, microtopography coatings maintained indiscriminate biocompatibility compared with Ti control. As a conclusion, a potential method to produce microtopography coatings with enhanced antibacterial activity and appropriate biocompatibility. There is magnificent benefit to apply this microtopography coating in the field of orthopaedic implants.

Author Contributions: Conceptualization, Z.P. and X.W.; methodology, Q.W.; software, Q.W.; validation, Z.H. and Q.W.; formal analysis, X.W.; investigation, X.W. and Z.H.; resources, Z.P.; data curation,

X.W.; writing—original draft preparation, X.W.; writing—review and editing, H.A.; visualization, Z.P.; supervision, Z.P.; project administration, Z.P.; funding acquisition, Z.P. All authors have read and agreed to the published version of the manuscript.

Institutional Review Board Statement: Not applicable.

Informed Consent Statement: Not applicable.

Data Availability Statement: Not applicable.

Conflicts of Interest: The authors report no conflict of interest in this work.

References

1. Kaur, M.; Singh, K. Review on titanium and titanium based alloys as biomaterials for orthopaedic applications. *Mater. Sci. Eng. C* **2019**, *102*, 844–862. [CrossRef] [PubMed]
2. Arciola, C.R.; Campoccia, D.; Montanaro, L. Implant infections: Adhesion, biofilm formation and immune evasion. *Nat. Rev. Microbiol.* **2018**, *16*, 397–409. [CrossRef] [PubMed]
3. Reffuveille, F.; Josse, J.; Vallé, Q.; Gangloff, C.M.; Gangloff, S.C. Staphylococcus aureus Biofilms and their Impact on the Medical Field. *Rise Virulence Antibiot. Resist. Staphylococcus Aureus* **2017**, *11*, 187.
4. Chouirfa, H.; Bouloussa, H.; Migonney, V.; Falentin-Daudré, C. Review of titanium surface modification techniques and coatings for antibacterial applications. *Acta Biomater.* **2019**, *83*, 37–54. [CrossRef] [PubMed]
5. Zhang, X.-F.; Liu, Z.-G.; Shen, W.; Gurunathan, S. Silver Nanoparticles: Synthesis, Characterization, Properties, Applications, and Therapeutic Approaches. *Int. J. Mol. Sci.* **2016**, *17*, 1534. [CrossRef] [PubMed]
6. Bonilla-Gameros, L.; Chevallier, P.; Sarkissian, A.; Mantovani, D. Silver-based antibacterial strategies for healthcare-associated infections: Processes, challenges, and regulations. An integrated review. *Nanomed. Nanotechnol. Biol. Med.* **2020**, *24*, 102142. [CrossRef] [PubMed]
7. Niu, X.; Sun, L.; Zhang, X.; Sun, Y.; Wang, J. Fabrication and antibacterial properties of cefuroxime-loaded TiO2 nanotubes. *Appl. Microbiol. Biotechnol.* **2020**, *104*, 2947–2955. [CrossRef] [PubMed]
8. Cho, J.-W.; Kim, J.; Cho, W.-T.; Kent, W.T.; Kim, H.-J.; Oh, J.-K. Antibiotic coated hinged threaded rods in the treatment of infected nonunions and intramedullary long bone infections. *Injury* **2018**, *49*, 1912–1921. [CrossRef]
9. Liao, C.; Li, Y.; Tjong, S.C. Bactericidal and Cytotoxic Properties of Silver Nanoparticles. *Int. J. Mol. Sci.* **2019**, *20*, 449. [CrossRef]
10. Hernando-Amado, S.; Coque, T.M.; Baquero, F.; Martínez, J.L. Defining and combating antibiotic resistance from One Health and Global Health perspectives. *Nat. Microbiol.* **2019**, *4*, 1432–1442. [CrossRef]
11. Aksel, H.; Mahjour, F.; Bosaid, F.; Calamak, S.; Azim, A.A. Antimicrobial Activity and Biocompatibility of Antibiotic-Loaded Chitosan Hydrogels as a Potential Scaffold in Regenerative Endodontic Treatment. *J. Endod.* **2020**, *46*, 1867–1875. [CrossRef] [PubMed]
12. Jeong, W.-S.; Kwon, J.-S.; Lee, J.-H.; Uhm, S.-H.; Choi, E.H.; Kim, K.-M. Bacterial attachment on titanium surfaces is dependent on topography and chemical changes induced by nonthermal atmospheric pressure plasma. *Biomed. Mater.* **2017**, *12*, 045015. [CrossRef] [PubMed]
13. Valle, J.; Burgui, S.; Langheinrich, D.; Gil, C.; Solano, C.; Toledo-Arana, A.; Helbig, R.; Lasagni, A.; Lasa, I. Evaluation of Surface Microtopography Engineered by Direct Laser Interference for Bacterial Anti-Biofouling. *Macromol. Biosci.* **2015**, *15*, 1060–1069. [CrossRef] [PubMed]
14. Wang, L.; Chen, W.; Terentjev, E. Effect of micro-patterning on bacterial adhesion on polyethylene terephthalate surface. *J. Biomater. Appl.* **2015**, *29*, 1351–1362. [CrossRef] [PubMed]
15. Yang, M.; Ding, Y.; Ge, X.; Leng, Y. Control of bacterial adhesion and growth on honeycomb-like patterned surfaces. *Colloids Surf. B Biointerfaces* **2015**, *135*, 549–555. [CrossRef] [PubMed]
16. Ge, X.; Leng, Y.; Lu, X.; Ren, F.; Wang, K.; Ding, Y.; Yang, M. Bacterial responses to periodic micropillar array. *J. Biomed. Mater. Res. Part A* **2015**, *103*, 384–396. [CrossRef]
17. Mitik-Dineva, N.; Wang, J.; Truong, V.K.; Stoddart, P.R.; Alexander, M.R.; Albutt, D.J.; Fluke, C.; Crawford, R.J.; Ivanova, E.P. Bacterial attachment on optical fibre surfaces. *Biofouling* **2010**, *26*, 461–471. [CrossRef]
18. Lee, J.; Pascall, M.A. Effect of micro—Pattern topography on the attachment and survival of foodborne microorganisms on food contact surfaces. *J. Food Saf.* **2017**, *38*, e12379. [CrossRef]
19. Vasudevan, R.; Kennedy, A.J.; Merritt, M.; Crocker, F.H.; Baney, R.H. Microscale patterned surfaces reduce bacterial fouling-microscopic and theoretical analysis. *Colloids Surf. B Biointerfaces* **2014**, *117*, 225–232. [CrossRef]

20. Jaggessar, A.; Shahali, H.; Mathew, A.; Yarlagadda, P.K.D.V. Bio-mimicking nano and micro-structured surface fabrication for antibacterial properties in medical implants. *J. Nanobiotechnol.* **2017**, *15*, 64. [CrossRef] [PubMed]

21. Chung, K.K.; Schumacher, J.F.; Sampson, E.M.; Burne, R.A.; Antonelli, P.J.; Brennan, A.B. Impact of engineered surface microtopography on biofilm formation of Staphylococcus aureus. *Biointerphases* **2007**, *2*, 89–94. [CrossRef] [PubMed]

22. Dickson, M.N.; Liang, E.I.; Rodriguez, L.A.; Vollereaux, N.; Yee, A.F. Nanopatterned polymer surfaces with bactericidal properties. *Biointerphases* **2015**, *10*, 021010. [CrossRef] [PubMed]

23. Lee, S.W.; Phillips, K.S.; Gu, H.; Kazemzadeh-Narbat, M.; Ren, D. How microbes read the map: Effects of implant topography on bacterial adhesion and biofilm formation. *Biomaterials* **2020**, *268*, 120595. [CrossRef] [PubMed]

24. Jemat, A.; Ghazali, M.J.; Razali, M.; Otsuka, Y. Surface Modifications and Their Effects on Titanium Dental Implants. *BioMed Res. Int.* **2015**, *2015*, 791725. [CrossRef] [PubMed]

25. Li, X.; Qi, M.; Sun, X.; Weir, M.D.; Tay, F.; Oates, T.W.; Dong, B.; Zhou, Y.; Wang, L.; Xu, H.H. Surface treatments on titanium implants via nanostructured ceria for antibacterial and anti-inflammatory capabilities. *Acta Biomater.* **2019**, *94*, 627–643. [CrossRef] [PubMed]

26. Mrad, O.; Saunier, J.; Aymes-Chodur, C.; Rosilio, V.; Bouttier, S.; Agnely, F.; Aubert, P.; Vigneron, J.; Etcheberry, A.; Yagoubi, N. A multiscale approach to assess the complex surface of polyurethane catheters and the effects of a new plasma decontamination treatment on the surface properties. *Microsc. Microanal.* **2010**, *16*, 764–778. [CrossRef] [PubMed]

27. Morata, L.; Cobo, J.; Fernández-Sampedro, M.; Vasco, P.G.; Ruano, E.; Lora-Tamayo, J.; Somolinos, M.S.; Ruano, P.G.; Nieto, A.R.; Arnaiz, A.; et al. Safety and Efficacy of Prolonged Use of Dalbavancin in Bone and Joint Infections. *Antimicrob. Agents Chemother.* **2019**, *63*, e02280-18. [CrossRef] [PubMed]

28. de Oliveira, W.F.; Silva, P.; Silva, R.; Silva, G.; Machado, G.; Coelho, L.; Correia, M. Staphylococcus aureus and Staphylococcus epidermidis infections on implants. *J. Hosp. Infect.* **2018**, *98*, 111–117. [CrossRef] [PubMed]

29. Ortiz, A.D.C.; Fideles, S.O.M.; Pomini, K.T.; Reis, C.H.B.; Bueno, C.R.D.S.; Pereira, E.D.S.B.M.; Rossi, J.D.O.; Novais, P.C.; Pilon, J.P.G.; Junior, G.M.R.; et al. Effects of Therapy with Fibrin Glue combined with Mesenchymal Stem Cells (MSCs) on Bone Regeneration: A Systematic Review. *Cells* **2021**, *10*, 2323. [CrossRef] [PubMed]

30. Wang, Z.; Shen, X.; Yan, Y.; Qian, T.; Wang, J.; Sun, Q.; Jin, C. Facile fabrication of a PDMS @ stearic acid-Al(OH)3 coating on lignocellulose composite with superhydrophobicity and flame retardancy. *Appl. Surf. Sci.* **2018**, *450*, 387–395. [CrossRef]

31. Tuo, Y.; Chen, W.; Zhang, H.; Li, P.; Liu, X. One-step hydrothermal method to fabricate drag reduction superhydrophobic surface on aluminum foil. *Appl. Surf. Sci.* **2018**, *446*, 230–235. [CrossRef]

32. Li, C.; Yang, Y.; Yang, L.; Shi, Z.; Yang, P.; Cheng, G. In Vitro Bioactivity and Biocompatibility of Bio-Inspired Ti-6Al-4V Alloy Surfaces Modified by Combined Laser Micro/Nano Structuring. *Molecules* **2020**, *25*, 1494. [CrossRef] [PubMed]

33. Liu, Y.; Rui, Z.; Cheng, W.; Song, L.; Xu, Y.; Li, R.; Zhang, X. Characterization and evaluation of a femtosecond laser-induced osseointegration and an anti-inflammatory structure generated on a titanium alloy. *Regen. Biomater.* **2021**, *8*, rbab006. [CrossRef]

34. Dumas, V.; Guignandon, A.; Vico, L.; Mauclair, C.; Zapata, X.; Linossier, M.T.; Bouleftour, W.; Granier, J.; Peyroche, S.; Dumas, J.-C.; et al. Femtosecond laser nano/micro patterning of titanium influences mesenchymal stem cell adhesion and commitment. *Biomed. Mater.* **2015**, *10*, 055002. [CrossRef] [PubMed]

35. Long, J.; Pan, L.; Fan, P.; Gong, D.; Jiang, D.; Zhang, H.; Li, L.; Zhong, M. Cassie-State Stability of Metallic Superhydrophobic Surfaces with Various Micro/Nanostructures Produced by a Femtosecond Laser. *Langmuir* **2016**, *32*, 1065–1072. [CrossRef] [PubMed]

36. Pingle, H.; Wang, P.; Thissen, H.; Kingshott, P. Controlled Attachment of Pseudomonas aeruginosa with Binary Colloidal Crystal—Based Topographies. *Small* **2018**, *14*, e1703574. [CrossRef]

37. Wang, Y.; Domingues, J.F.D.S.; Subbiahdoss, G.; van der Mei, H.C.; Busscher, H.J.; Libera, M. Conditions of lateral surface confinement that promote tissue-cell integration and inhibit biofilm growth. *Biomaterials* **2014**, *35*, 5446–5452. [CrossRef] [PubMed]

38. Visai, L.; De Nardo, L.; Punta, C.; Melone, L.; Cigada, A.; Imbriani, M.; Arciola, C.R. Titanium oxide antibacterial surfaces in biomedical devices. *Int. J. Artif. Organs* **2011**, *34*, 929–946. [CrossRef]

39. Zhao, Q.-M.; Sun, Y.-Y.; Wu, C.-S.; Yang, J.; Bao, G.-F.; Cui, Z.-M. Enhanced osteogenic activity and antibacterial ability of manganese–titanium dioxide microporous coating on titanium surfaces. *Nanotoxicology* **2020**, *14*, 289–309. [CrossRef]

40. Souza, J.C.M.; Sordi, M.B.; Kanazawa, M.; Ravindran, S.; Henriques, B.; Silva, F.S.; Aparicio, C.; Cooper, L.F. Nano-scale modification of titanium implant surfaces to enhance osseointegration. *Acta Biomater.* **2019**, *94*, 112–131. [CrossRef]

41. Bharadwaz, A.; Jayasuriya, A.C. Recent trends in the application of widely used natural and synthetic polymer nanocomposites in bone tissue regeneration. *Mater. Sci. Eng. C* **2020**, *110*, 110698. [CrossRef] [PubMed]

42. Spriano, S.; Chandra, V.S.; Cochis, A.; Uberti, F.; Rimondini, L.; Bertone, E.; Vitale, A.; Scolaro, C.; Ferrari, M.; Cirisano, F.; et al. How do wettability, zeta potential and hydroxylation degree affect the biological response of biomaterials? *Mater. Sci. Eng. C* **2017**, *74*, 542–555. [CrossRef] [PubMed]

43. Dickinson, L.E.; Rand, D.R.; Tsao, J.; Eberle, W.; Gerecht, S. Data associated with: Endothelial cell responses to micropillar substrates of varying dimensions and stiffness. *J. Biomed. Mater. Res. Part A* **2012**, *100*, 1457–1466. [CrossRef] [PubMed]

44. Ochsner, M.; Textor, M.; Vogel, V.; Smith, M.L. Dimensionality controls cytoskeleton assembly and metabolism of fibroblast cells in response to rigidity and shape. *PLoS ONE* **2010**, *5*, e9445. [CrossRef] [PubMed]